Nanoscale

ROYAL SOCIETY OF CHEMISTRY

PAPER

View Article Online
View Journal | View Issue



Cite this: *Nanoscale*, 2021, **13**, 19049

# A phase-transfer catalyst-based nanoreactor for accelerated hydrogen sulfide bio-imaging†

Panfei Xing,‡[a,b] Yiming Niu,‡[a,c] Jiacheng Li,[a] Daping Xie,[a] Huiqun Zhou,[a] Jiaxi Chen,[a] Lei Dong *[c] and Chunming Wang *[a]

Hydrogen sulfide ($H_2S$) is an important signaling molecule in various biological processes; however, its real-time monitoring in living cells is hampered by long detection time for current fluorescent probes. To overcome this challenge, we designed a phase-transfer catalyst (PTC) approach to accelerate the reaction between the probe and the analyte by conjugating common fluorescent probes – mostly hydrophobic small molecules – with an amphiphilic PEG–PPG–PEG polymer, enabling the controllable assembly of $H_2S$ nanoprobes in an aqueous solution. The PEG block helps to establish a PTC microenvironment that endows the assembled nanoprobes with a significantly reduced detection time (3–10 min; *versus* 20–60 min for small-molecule probes). Based on this approach, we synthesised two nanoprobes of different wavelengths, **DS-Blue-nano** and **DN-Green-nano**, which can sensitively detect $H_2S$ in living macrophage cells with bright fluorescence starting at as early as 7 min and reaching stability at 15 min. These data suggest PTC-based nanoprobes as a new and generic approach for constructing sensitive fluorescent probes for the real-time imaging of $H_2S$, and perhaps other molecules in future, under biological conditions.

Received 29th July 2021,
Accepted 25th October 2021

DOI: 10.1039/d1nr04931c

rsc.li/nanoscale



## Introduction

Hydrogen sulfide ($H_2S$) is a versatile gaseous signal molecule produced endogenously through both enzymatic and non-enzymatic processes in living systems.[1] $H_2S$ plays an essential role in vascular smooth muscle relaxation, neurotransmitter regulation, redox status modulation and many other physiological processes.[2] Its abnormal changes are associated with Alzheimer's disease, diabetes, and cardiovascular diseases.[3] Developing chemical tools to detect $H_2S$ in subcellular microenvironments will provide powerful insight into understanding pathogenic mechanisms. Nevertheless, despite the development of fluorescent probes for $H_2S$ for decades, one substantial and common challenge still facing real-time $H_2S$ monitoring in living cells is particularly a long detection time (>20 min) in aqueous solutions.[4–8] Since metabolic reactions take place fast in the physiological system, such long detection times may easily lead to artifacts,[9] *e.g.*, unintended detection of re-synthesized or cleared $H_2S$. Therefore, shortening the detection time to realise 'real-time' detection (*e.g.*, within 5 min) of $H_2S$ in living systems is critical for understanding the genuine action of this gaseous molecule in subcellular microenvironments.[9]

The mechanisms of reaction-based fluorescent probes for detecting $H_2S$ mainly include: (i) disulfide exchange, (ii) aryl nitro thiolysis and (iii) azide reduction,[10–13] all based on the high reducibility and nucleophilicity of $H_2S$. However, in aqueous solutions, $H_2S$ is primarily in the monoanionic form, $HS^-$.[14] Moreover, fluorescent probes are typically constructed from hydrophobic dyes with large π-conjugation. The hydrophobic probes and hydrophilic analyte ($HS^-$) may have low reaction efficiency, which is a possible reason for the long detection time. Although co-organic solvents are commonly used to solve this issue, they can only be used in preliminary tests without living cells due to their obvious toxicity to cells.

To solve this problem, we proposed the conjugation of common fluorescent probes for $H_2S$ – mostly hydrophobic small molecules – with an amphiphilic triblock poly(ethylene glycol)–poly(propylene glycol)–poly(ethylene glycol) (PEG–PPG–PEG) copolymer. In aqueous solutions, the polymer-probe conjugates self-assemble into nanoparticles *via* the micelle packing mechanism.[15] Here, PEG plays the role of a phase transfer catalyst (PTC)[16–19] to increase the reaction efficiency between the hydrophobic probe and hydrophilic

[a]*State Key Laboratory of Quality Research in Chinese Medicine, Institute of Chinese Medical Sciences, University of Macau, Taipa, Macau SAR, China. E-mail: cmwang@umac.mo*
[b]*Key Laboratory of Natural Medicine and Immuno-Engineering, Henan University, Kaifeng 475004, People's Republic of China*
[c]*State Key Laboratory of Pharmaceutical Biotechnology, School of Life Sciences, Nanjing University, Nanjing, Jiangsu 210023, China. E-mail: leidong@nju.edu.cn*
†Electronic supplementary information (ESI) available. See DOI: 10.1039/d1nr04931c
‡These authors contributed equally.

$HS^-$, while PPG and probes offer hydrophobic units. In this study, we set out to construct the PTC-based nanoprobes, validate their efficiency in detecting $H_2S$ in aqueous solutions, and finally assess their potential in living cell culture. Our data suggest that the PTC-based nanoprobes were more sensitively and effectively image $H_2S$ than conventional probes, thus shortening the detection time from ~20–60 min to ~3–10 min (Scheme 1).

## Experimental methods

### Materials and instruments

All the solvents and chemical reagents were from commercial sources, analytical grade and used without further purification. $^1$H NMR and $^{13}$C NMR spectra were recorded on a Bruker 600 MHz AVANCE III spectrometer with chemical shifts reported in ppm at room temperature. DLS analyses were performed using a Malvern Zetasizer Nano ZS (UK). Absorption spectra were collected on a HACH DR6000 UV/VIS Spectrophotometer (USA). Fluorescence spectra were obtained on a Thermo Scientific Lumina Fluorescence Spectrometer (USA). The fluorescence imaging of cells was performed using a Leica DMi8 fluorescence microscope. Each experiment was observed using 325–375 nm exciter, 435–485 nm emitter for the blue channel, and 460–500 nm exciter, 512–542 nm emitter for the green channel.

### Preparation of nanoprobes

Probe–polymer was dissolved in THF (50 μL) and swiftly added into an aqueous solution (5 mL) under ultrasound. Nitrogen was then used to dislodge THF, obtaining an aqueous solution of the nanoprobe.

### Characterization of polymeric micelles

The mean particle size and polydispersity index (PDI) of nanoreactors were determined by dynamic light scattering (DLS). The polymeric micelle concentrations were kept at 0.5 mg $mL^{-1}$ for DLS measurements. The measurements were performed in triplicate for each sample. The nanoparticle tracking analysis technique (NanoSight NS500) was applied to visualize the nanoprobe dispersed in an aqueous solution and quantified the relevant number weighted distributions.

## Results and discussion

First, our data confirmed a common concern that fluorescent probes reacted to the analyte $H_2S$ much slower in an aqueous solution than in an organic co-solvent system. We examined the response of common fluorescent probes to $H_2S$ in absolute phosphate buffered saline (PBS; 10 mM, pH 7.4) or mixtures of ethanol in PBS (10%, 20%, and 30%, respectively, v/v). As shown in Fig. 1, we synthesized three fluorescent probes **DS-Blue**, **DN-Green**, and **AZ-Green**, representing the three detection principles of disulfide exchange, aryl nitro thiolysis, and azide reduction, respectively.[20–22] With the addition of 20 equivalents of $H_2S$ ($Na_2S$ as the donor) to each solution of the three probes in absolute PBS (10 mM, 7.4), reaction times of 22 min, 30 min, and 60 min were observed. However, it decreased with the gradual increase in ethanol from 10% to 30% in a PBS solution (10 mM, pH 7.4, v/v). Also, a higher percentage of ethanol always meant a shorter reaction time. These results suggested that the organic co-solvent solution accelerated the reaction time, agreeing with our assumption that the probe hydrophobicity could account for their low reactive efficiency for the hydrophilic $HS^-$.

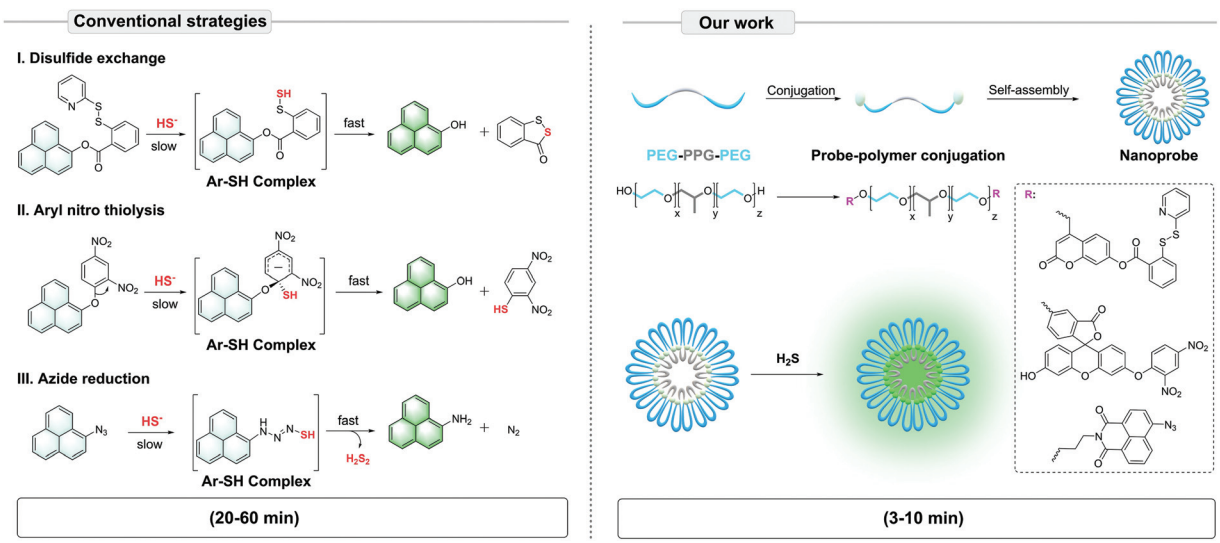


Scheme 1 Illustration of the PTC-based approach to construct self-assembled nanoprobes for $H_2S$, based on conventional strategies of fluorescent nanoprobe development.

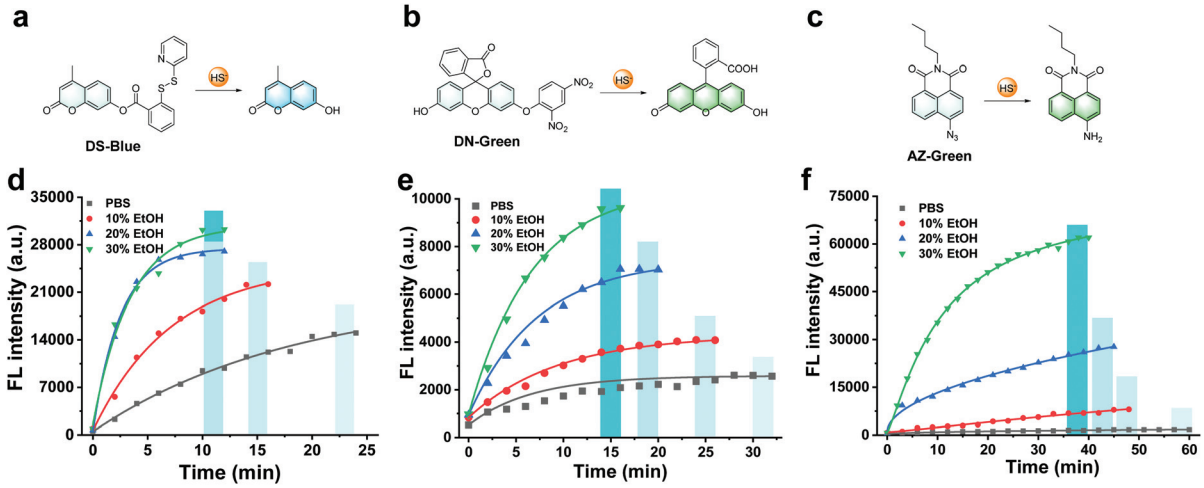


Fig. 1 Co-solvent effect on the reaction time of fluorescent probes to $H_2S$. (a–c) Chemical structure and the detection mechanism of **DS-Blue**, **DN-Green**, and **AZ-Green**. (d) Time course of **DS-Blue** (10 μM) with the addition of 20 equivalents $H_2S$. (e) Time course of **DN-Green** (10 μM) with the addition of 20 equivalents $H_2S$. (f) Time course of **AZ-Green** (10 μM) with the addition of 20 equivalents $H_2S$. Solutions are PBS, 10% ethanol, 20% ethanol, and 30% ethanol in PBS (10 mM, pH 7.4, v/v), respectively.

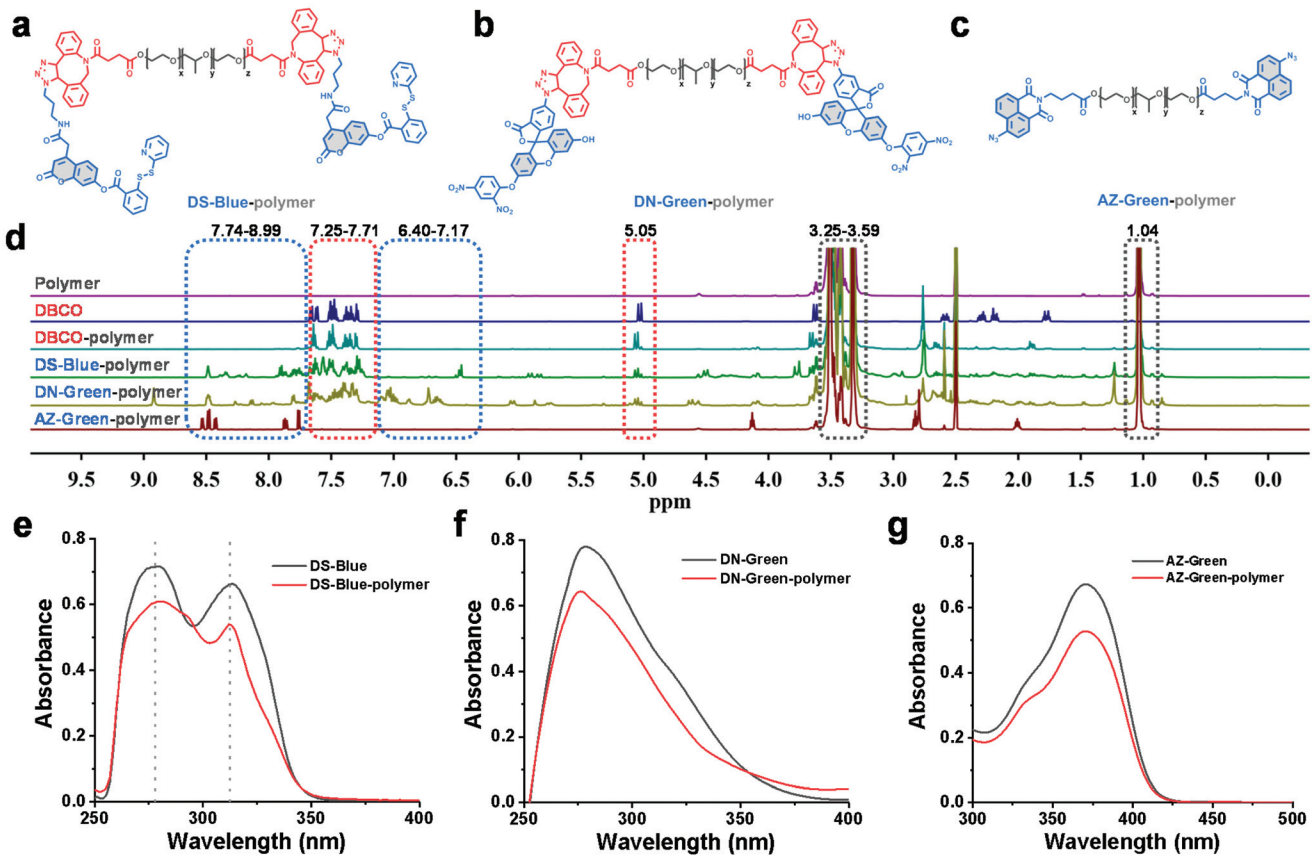


Fig. 2 Synthesis and characterization of probe–polymer conjugates. (a–c) Chemical structure of the fluorescent probe–polymer conjugates, **DS-Blue**-polymer, **DN-Green**-polymer, and **AZ-Green**-polymer. (d) $^1H$ NMR spectra of polymer, DBCO, DBCO-polymer, **DS-Blue**-polymer, **DN-Green**-polymer, and **AZ-Green**-polymer in DMSO-$d_6$. (e–g) Absorbance of **DS-Blue**, **DS-Blue**-polymer, **DN-Green**, **DN-Green**-polymer, **AZ-Green**, and **AZ-Green**-polymer in DMSO.

To form a self-assembled nanoreactor of PEG in aqueous solutions, the amphiphilic copolymer PEG–PPG–PEG was selected as the key conjugation unit, which has hydrophilic PEG blocks and hydrophobic PPG blocks.[23] **DS-Blue**-polymer and **DN-Green**-polymer conjugations were obtained by grafting **DS-Blue-Azido** and **DN-Green-Azido** onto PEG–PPG–PEG in two steps: first to produce dibenzocyclooctyne (DBCO)-polymer grafted by the EDC/NHS coupling chemistry reaction between DBCO and PEG–PPG–PEG, followed by grafting of **DS-Blue-Azido** and **DN-Green-Azido** onto the DBCO-polymer through a click reaction. AZ-Green was obtained directly by the coupling chemistry reaction between **AZ-Green-COOH** and PEG–PPG–PEG. The final structures of **DS-Blue**-polymer, **DN-Green**-polymer, and **AZ-Green**-polymer are shown in Fig. 2a–c. The conjugate formation of the DBCO-polymer and probe–polymer was confirmed by Fourier-transform infrared spectroscopy (FT-IR) and $^1$H NMR spectroscopy (Fig. 2d). FT-IR spectra showed a markedly enhanced absorption at 1735 cm$^{-1}$ (C═O stretch) and decreased signal at 3450 cm$^{-1}$ (O–H stretch), confirming the successful modification of hydroxyl groups on the polymer chain are substituted by carbonyl groups and convert to esters, compared with the initial polymer PEG–PPG–PEG (Fig. S30†). The $^1$H NMR spectrum of DBCO-polymer showed two types of characteristic peaks at 1.04, and 3.25–3.59 (attributed to PEG–PPG–PEG, indicated by black box lines in the spectrum) and 5.05 and 7.25–7.71 (attributed to DBCO, red box lines). In addition to these two kinds of characteristic peaks, **DS-Blue**-polymer and **DN-Green**-polymer showed novel peaks at 6.40–7.17 and 7.74–8.99 (attributed to the aromatic peaks of **DS-Blue-Azido** and **DN-Green-Azido**, blue box lines). The **AZ-Green**-polymer showed combined peaks of PEF-PPG-PEG (black box lines) and **AZ-Green-COOH** (blue box

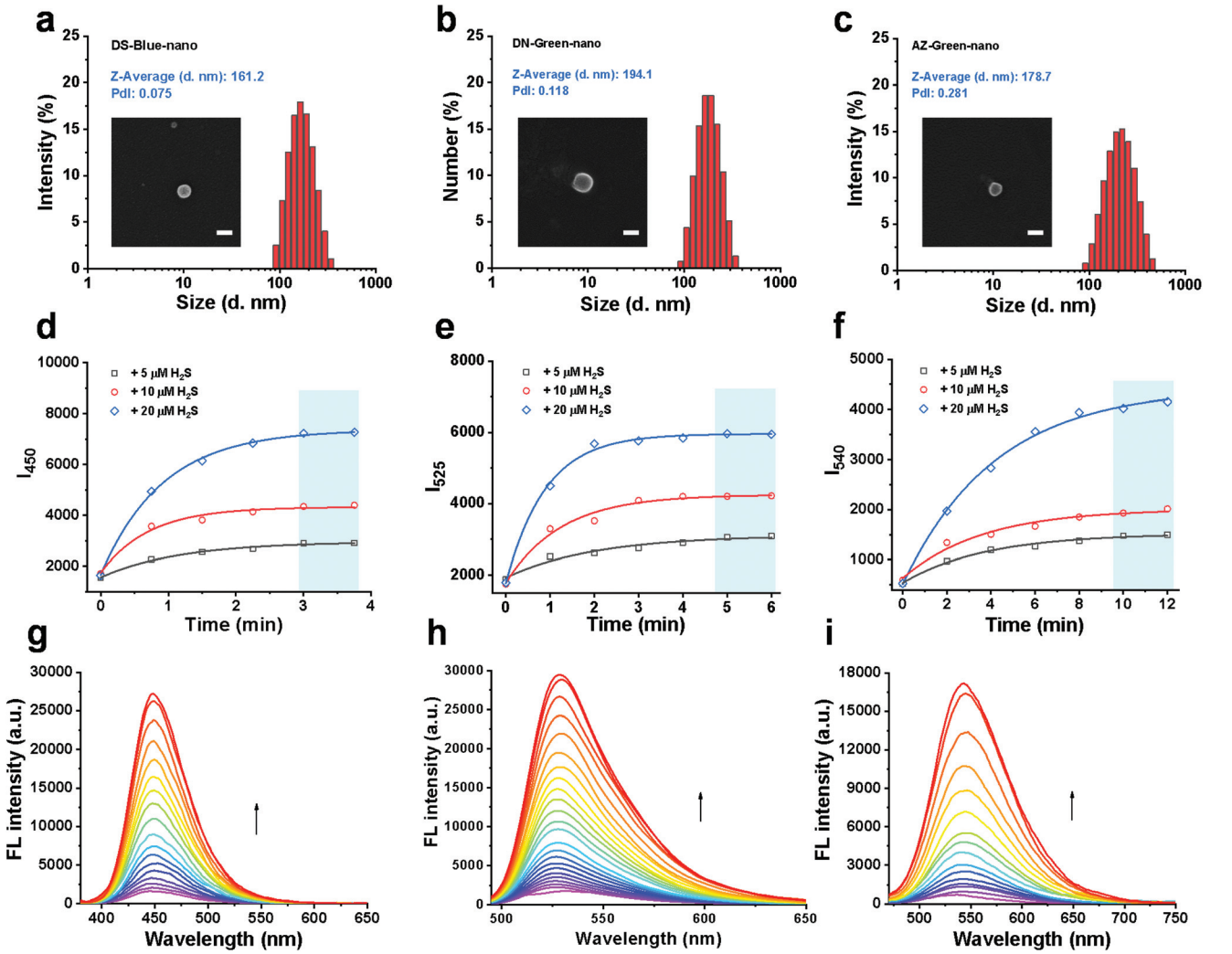


**Fig. 3** Construction and validation of PTC-based nanoprobes of **DS-Blue-Nano**, **DN-Green-Nano**, and **AZ-Green-Nano**. (a–c) Particle size distributions of **DS-Blue-Nano**, **DN-Green-Nano**, and **AZ-Green-Nano** measured by DLS, PdI < 0.3. The insets in Fig. 3a–c show the SEM images of the samples and scale bars correspond to 200 nm; (d–f) time-course of **DS-Blue-Nano**, **DN-Green-Nano**, and **AZ-Green-Nano** (10 μM for each) with the addition of $H_2S$ (5 μM, black; 10 μM, red; 20 μM, blue) in PBS (10 mM, pH 7.4); (g–i) fluorescent titration of **DS-Blue-Nano**, **DN-Green-Nano**, and **AZ-Green-Nano** (10 μM for each) in response to different concentrations of $H_2S$ in PBS (10 mM, pH 7.4).

lines). These peak changes confirmed successful conjugation between fluorescent probes and PEG–PPG–PEG. Also, the absorbance of the probe–polymer conjugation matched well with the characteristic peaks of the free probe, indicating successful conjugation between the fluorescent probes and PEG–PPG–PEG polymer consistent with FT-IR and $^1$H NMR results (Fig. 2e–g).

The molar concentrations of fluorescent probes in the conjugates, **DS-Blue**-polymer, **DN-Green**-polymer, and **AZ-Green**-polymer (1 mg mL$^{-1}$ for each group in DMSO) were calculated by the standard curve of each free probe in DMSO to be 40.23, 39.58, and 25.02 μM, respectively (Fig. S1–3†). Nanoprobes were prepared through simple nanoprecipitation. Dynamic light scattering (DLS) revealed that the nanoprobes **DS-Blue-Nano**, **DN-Green-Nano**, and **AZ-Green-Nano** were successfully prepared and presented narrow size distributions with average diameters of 161.2, 194.1, and 178.7 nm, respectively (Fig. 3a). From the representative SEM image of **DS-Blue-Nano**, **DN-Green-Nano**, and **AZ-Green-Nano**, the size of nanoprobes was ~200 nm (Fig. S4a†), consistent with the DLS data. Similar results were further confirmed by the nanoparticle tracking analysis and the relevant number weighted distributions (Fig. S4b†). Next, we examined the fluorescent response of the nanoprobes towards $H_2S$. With the addition of 5, 10, or 20 μM $H_2S$, the time-course of **DS-Blue-Nano**, **DN-Green-Nano**, and **AZ-Green-Nano** (10 μM for each) showed that the fluorescence intensity reached a steady state after 3, 5, and 10 min, respectively (Fig. 3d–f). Compared with free fluorescent probes of **DS-Blue**, **DN-Green**, and **AZ-Green**, the constructed nanoprobes showed a significantly reduced reaction time. Also, a non-covalent complex formed by the addition of PEG derivatives was found to produce similar results in the detection of $H_2S$ from literature reports.[24–26] All these data confirmed the function of PEG in accelerating the reaction of the probe to $H_2S$. In addition, the fluorescence intensity of **DS-Blue-Nano**, **DN-Green-Nano**, and **AZ-Green-Nano** in response to $H_2S$ is dose-dependent (Fig. 3g–i). Also, the fluorescence enhancement of **DS-Blue-Nano**, **DN-Green-Nano**, and **AZ-Green-Nano** to $H_2S$ shows excellent linear responses up to 75 μM, 100 μM, and 85 μM, respectively (Fig. S5–7†). The detection limits (LODs) of **DS-Blue-nano**, **DN-Green-nano**, and **AZ-Green-nano** for $H_2S$ were calculated to be 20.3 nM, 10.2 nM, and 36.0 nM, respectively, using the equation $3\delta/k$.[27–29] The limits of quantification (LOQ) of **DS-Blue-nano**, **DN-Green-nano**, and **AZ-Green-nano** for $H_2S$ were calculated to be 67.7 nM, 33.9 nM, and 119.9 nM, respectively.[30] To test the selectivity of these nanoprobes to $H_2S$ over other analytes, we had chosen $Na^+$, $K^+$, $Cl^-$, $Br^-$, $CO_3^{2-}$, $SO_4^{2-}$, $H_2PO_4^-$, $CH_3COO^-$, $HCO_3^-$, $NO_3^-$, Cys, Hcy, and GSH (200 μM for each) as interferents. As shown in Fig. S8,† almost no fluorescent change was found in the presence of these analytes, Implying that these analytes did not interfere with the detection process of **DS-Blue-nano**, **DN-Green-nano**, and **AZ-Green-nano** for $H_2S$.

We next examined the thermal behaviour of the free probes and nanoprobes (Fig. 4a–c). The thermal activation energies of **DS-Blue-Nano**, **DN-Green-Nano**, and **AZ-Green-Nano** were calculated from the fitting of the *Arrhenius* plot as 11.49 ± 0.49, 10.08 ± 1.62, and 6.32 ± 0.11 kJ mol$^{-1}$ (indicated with red bar), respectively. In contrast, these were calculated to be 50.37 ± 3.82, 39.45 ± 3.53, and 41.17 ± 5.16 kJ mol$^{-1}$ for **DS-Blue**, **DN-Green**, and **AZ-Green**, respectively (Fig. 4d). In the latter case, they all showed higher activation energies than nanoreactors. In the Arrhenius equation, the activation energy is defined as the minimum energy required to initiate a chemical

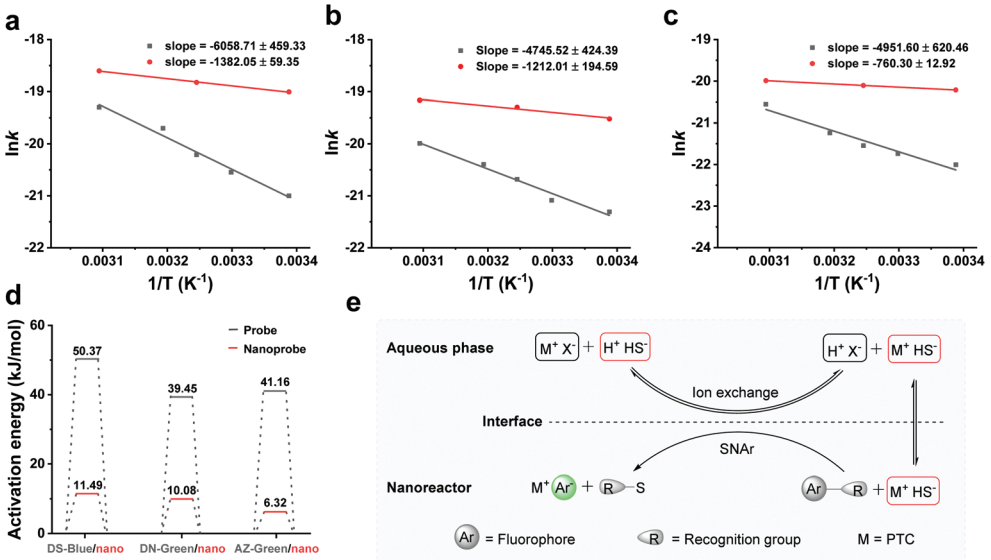


Fig. 4 Kinetic study of **DS-Blue-Nano**, **DN-Green-Nano**, and **AZ-Green-Nano** and proposed PTC mechanism of the nanoreactor to $H_2S$. (a–c) Arrhenius plot of **DS-Blue**, **DS-Blue-Nano**, **DN-Green**, **DN-Green-Nano**, **AZ-Green**, and **AZ-Green-Nano**; (d) The thermal activation energy of **DS-Blue**, **DS-Blue-Nano**, **DN-Green**, **DN-Green-Nano**, **AZ-Green**, and **AZ-Green-Nano**; (e) Proposed PTC mechanism of the nanoreactor in accelerating the reaction of probes to $H_2S$.

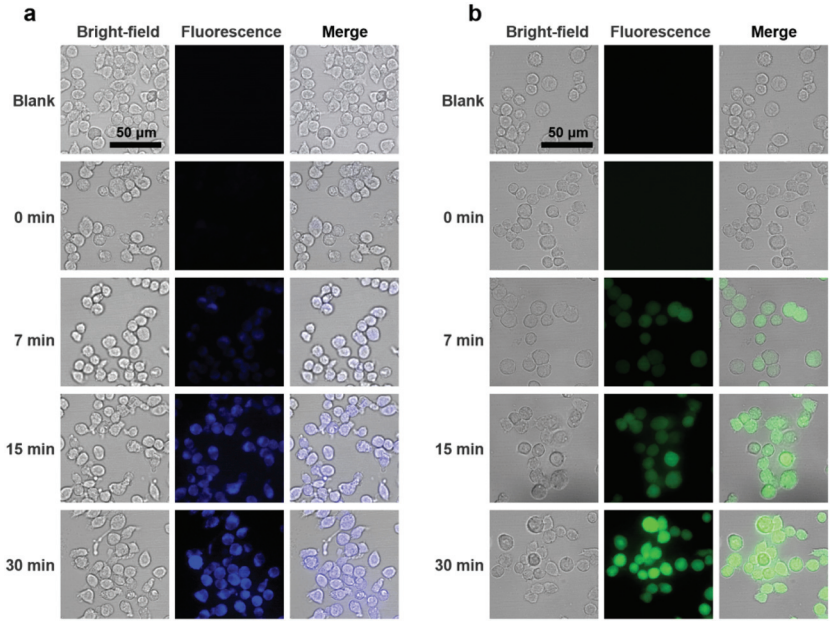


**Fig. 5** Detection of $H_2S$ by **DS-Blue-Nano** and **DN-Green-Nano** in living macrophage cells. Cells were treated with $Na_2S$ (100 μM) to generate exogenous $H_2S$, untreated cells were used as control. The cells were then incubated with **DS-Blue-Nano** (10 μM, as a) or **DN-Green-Nano** (10 μM, as b). The photos were taken under a fluorescent microscope. Scale bar: 50 μm.

reaction. Based on these findings, we proposed that PEG as a PTC in nanoreactors allows the reaction of the hydrophobic fluorescent probes and hydrophilic $HS^-$ of two different immiscible phases *via* facilitating the transfer of $HS^-$ from the interface. And the catalyst regenerates again after the reaction is complete, continuing the catalytic cycle (Fig. 4e). PEG undergoes dissolution in the aqueous phase and anion exchange with $HS^-$ dissolved in the aqueous phase. The formed ion pair ($M^+HS^-$) then passes through the liquid–liquid interface and undergoes diffusion from the interface to the lipophilic phase. In the lipophilic phase, the anion from the ion pair ($M^+HS^-$) is nucleophilic, and reacts with the organic fluorescent probes with lower reaction barrier and forms subsequent fluorescent products.[31,32]

To explore the potential applications of the PTC-based nanoprobes in living cells, we used self-assembled **DS-Blue-nano** and **DN-Green-nano** as proof-of-concept model probes to image $H_2S$ in living murine macrophages (RAW 264.7) and breast cancer cell line (MCF-7). First, cell viability tests showed that both nanoprobes exhibited high biocompatibility at a dose of up to 40 μM in RAW 264.7 cells and MCF-7 cells after a 24 h incubation period (Fig. S10†).[33] Then, cell imaging experiments demonstrated that **DS-Blue-nano** and **DN-Green-nano** afforded bright fluorescence signals in blue and green channels from as early as 7 min after their addition to the cells pretreated with $H_2S$ for 1 h (Fig. 5 and Fig. S11†). The fluorescence signals became stable at 15 min and showed no significant changes after a longer incubation time (up to 30 min). Also, **DS-Blue-nano** and **DN-Green-nano** showed similar tendency for fast detection in these two cells. These results highlighted the high sensitivity of PTC-based nanoprobes and rapid detection of $H_2S$ in living cells.

## Conclusions

In summary, we have developed an effective and generic approach to increase the reaction speed for fluorescent probes to detect $H_2S$, enabling accelerated, sensitive, and real-time imaging of $H_2S$ in living cells. The core of this approach entails the transformation of common $H_2S$ fluorescent probes into phase-transfer catalyst-based nanoprobes, through the chemical conjugation of the probes with an amphiphilic polymer that induces self-assembly into colloidal structures. This nanoreactor approach provides a straightforward and effective solution to reduce the activation barrier typically existing in $H_2S$ fluorescent probes and can be applied to probes designed from different reaction principles, hence showing the potential to overcome the long-lasting, common challenge for the bioimaging of $H_2S$ – an important physiological gaseous molecule.

## Author contributions

C.W., L.D., P.X., and Y.N. designed the study. P.X. performed major chemical experiments. Y.N performed major biological experiments. J.L., D.X., H.Z., and J.C. performed experiments. P.X., Y.N., and C.W. drafted the manuscript. C.W. provided

 

funding supports. All authors contributed to data analysis and manuscript drafting.

## Conflicts of interest

There are no conflicts to declare.

## Acknowledgements

This study was funded by the Science and Technology Development Fund, Macau SAR (File no. 0018/2019/AFJ, 0097/2019/A2), the University of Macau Research Committee (MYRG2019-00080-ICMS), the National Natural Science Foundation of China (32000935) and China Postdoctoral Science Foundation funded project (Special Program, 2020TQ0140). We thank Ms Yuwei Li for her technical assistance in the process of manuscript revision.

## Notes and references

1 H. Peng, Y. Cheng, C. Dai, A. L. King, B. L. Predmore, D. J. Lefer and B. Wang, *Angew. Chem., Int. Ed.*, 2011, **50**, 9672–9675.
2 Y. F. Njie-Mbye, C. Opere, M. Chitnis and S. Ohia, *Front. Physiol.*, 2012, **3**, 295.
3 J.-y. Zhang, Y.-p. Ding, Z. Wang, Y. Kong, R. Gao and G. Chen, *Med. Gas Res.*, 2017, **7**, 113.
4 J. Kang, F. Huo and C. Yin, *Dyes Pigm.*, 2017, **146**, 287–292.
5 Y. L. Pak, J. Li, K. C. Ko, G. Kim, J. Y. Lee and J. Yoon, *Anal. Chem.*, 2016, **88**, 5476–5481.
6 Y. Ji, L.-J. Xia, L. Chen, X.-F. Guo, H. Wang and H.-J. Zhang, *Talanta*, 2018, **181**, 104–111.
7 C. S. Park, T. H. Ha, S.-A. Choi, D. N. Nguyen, S. Noh, O. S. Kwon, C.-S. Lee and H. Yoon, *Biosens. Bioelectron.*, 2017, **89**, 919–926.
8 A. R. Lippert, E. J. New and C. J. Chang, *J. Am. Chem. Soc.*, 2011, **133**, 10078–10080.
9 X. Jiang, L. Wang, S. L. Carroll, J. Chen, M. C. Wang and J. Wang, *Antioxid. Redox Signal.*, 2018, **29**, 518–540.
10 W. Xuan, C. Sheng, Y. Cao, W. He and W. Wang, *Angew. Chem., Int. Ed.*, 2012, **51**, 2282–2284.
11 D. A. Jose, R. Sakla, N. Sharma, S. Gadiyaram, R. Kaushik and A. Ghosh, *ACS Sens.*, 2020, **5**, 3365–3391.
12 H. Li, Y. Fang, J. Yan, X. Ren, C. Zheng, B. Wu, S. Wang, Z. Li, H. Hua, P. Wang and D. Li, *Trends Anal. Chem.*, 2021, **134**, 116117.
13 F. Yu, X. Han and L. Chen, *Chem. Commun.*, 2014, **50**, 12234–12249.
14 V. S. Lin, W. Chen, M. Xian and C. J. Chang, *Chem. Soc. Rev.*, 2015, **44**, 4596–4618.
15 S. Y. Lee, Y. Lee, S. Y. Chae, T. G. Park and C. H. Ahn, *Macromol. Chem. Phys.*, 2010, **211**, 692–697.
16 C. Mukhopadhyay, P. K. Tapaswi and R. J. Butcher, *Org. Biomol. Chem.*, 2010, **8**, 4720–4729.
17 G. D. Yadav and B. G. Motirale, *Org. Process Res. Dev.*, 2009, **13**, 341–348.
18 D. E. Bergbreiter, J. Tian and C. Hongfa, *Chem. Rev.*, 2009, **109**, 530–582.
19 D. E. Bergbreiter, *Chem. Rev.*, 2002, **102**, 3345–3384.
20 B. Peng, W. Chen, C. Liu, E. W. Rosser, A. Pacheco, Y. Zhao, H. C. Aguilar and M. Xian, *Chem. – Eur. J.*, 2014, **20**, 1010–1016.
21 Z. Wu, D. Liang and X. Tang, *Anal. Chem.*, 2016, **88**, 9213–9218.
22 H.-Y. Liu, M. Zhao, Q.-L. Qiao, H.-J. Lang, J.-Z. Xu and Z.-C. Xu, *Chin. Chem. Lett.*, 2014, **25**, 1060–1064.
23 L. Yu and J. Ding, *Chem. Soc. Rev.*, 2008, **37**, 1473–1481.
24 R. Wang, X. Gu, Q. Li, J. Gao, B. Shi, G. Xu, T. Zhu, H. Tian and C. Zhao, *J. Am. Chem. Soc.*, 2020, **142**, 15084–15090.
25 B. Shi, X. Gu, Z. Wang, G. Xu, Q. Fei, J. Tang and C. Zhao, *ACS Appl. Mater. Interfaces*, 2017, **9**, 35588–35596.
26 R. Wang, K. Dong, G. Xu, B. Shi, T. Zhu, P. Shi, Z. Guo, W.-H. Zhu and C. Zhao, *Chem. Sci.*, 2019, **10**, 2785–2790.
27 S. Gong, Z. Zheng, X. Guan, S. Feng and G. Feng, *Anal. Chem.*, 2021, **93**, 5700–5708.
28 S. Pei, J. Li, C. Zhang, W. Liang, G. Zhang, L. Shi, W. Wang, S. Shuang and C. Dong, *Analyst*, 2021, **146**, 2138–2143.
29 Z.-H. Zhang, S. Li, Y. Yan, J. Qu and J.-Y. Wang, *New J. Chem.*, 2021, **45**, 9756–9760.
30 P. Sukhavattanakul and H. Manuspiya, *Carbohydr. Polym.*, 2021, **254**, 117442.
31 D. O. Katole and G. D. Yadav, *Mol. Catal.*, 2019, **466**, 112–121.
32 N. Patel, R. Sood and P. V. Bharatam, *Chem. Rev.*, 2018, **118**, 8770–8785.
33 C. Wang, G. N. Adrianus, N. Sheng, S. Toh, Y. Gong and D.-A. Wang, *Biomaterials*, 2009, **30**(36), 6986–6995.